iScience

CellPress
OPEN ACCESS

Article

# Selective polypeptide ligand binding to the extracellular surface of the transmembrane domains of the class B GPCRs GLP-1R and GCGR

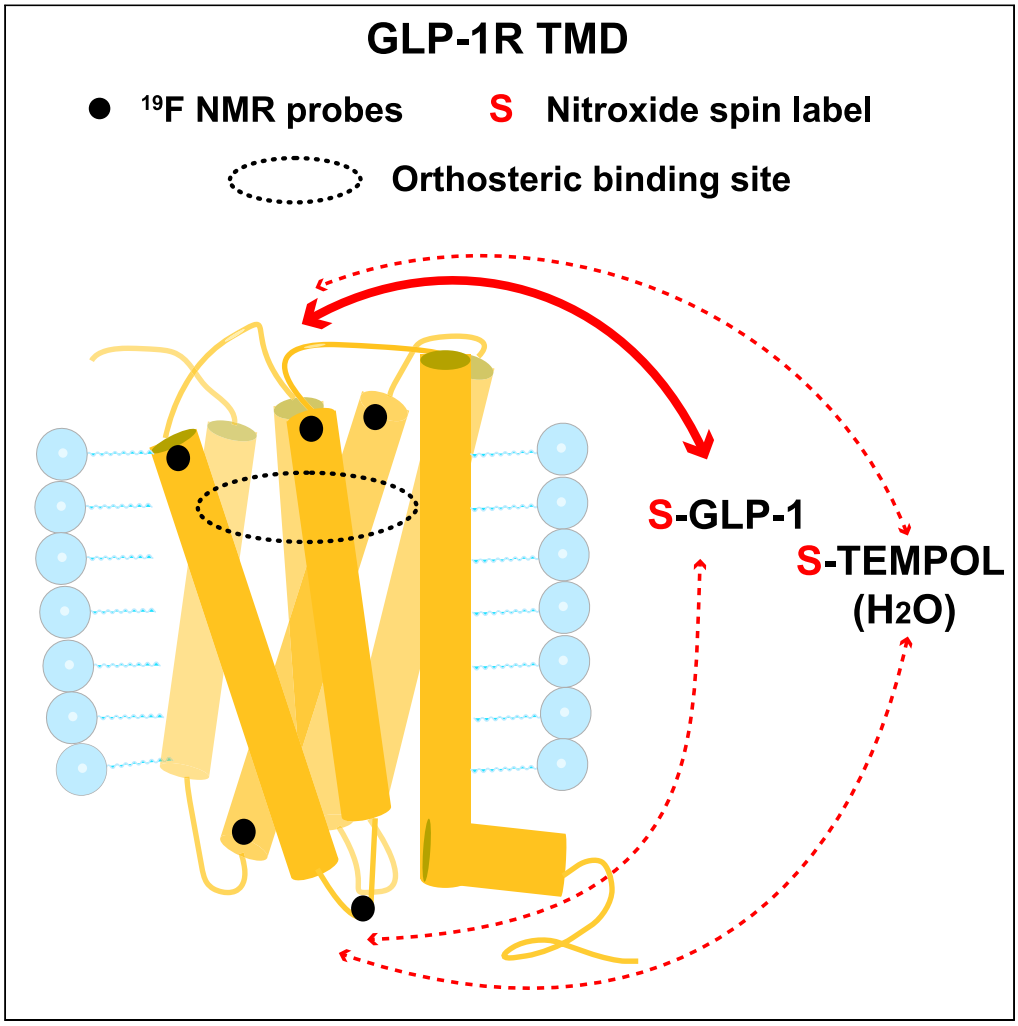


Huixia Wang, Wanhui Hu, Tiandan Xu, Ya Yuan, Dongsheng Liu, Kurt Wüthrich

liudsh@shanghaitech.edu.cn

## Highlights

Dual labeling: $^{19}$F on receptors and nitroxide spin labels on polypeptides

Polypeptides selectively interact with the extracellular surface of GLP-1R and GCGR

Ligand selectivity for the extracellular surface preserved in TMD of GLP-1R and GCGR

Cross-reactivity among GLP-1R, GCGR, glucagon and GLP-1 observed

Wang et al., iScience 26, 106918
June 16, 2023 
https://doi.org/10.1016/j.isci.2023.106918

iScience

CellPress
OPEN ACCESS

Article

# Selective polypeptide ligand binding to the extracellular surface of the transmembrane domains of the class B GPCRs GLP-1R and GCGR

Huixia Wang,[1,2,3,4] Wanhui Hu,[1,6] Tiandan Xu,[1,2,3,4,7] Ya Yuan,[1,8] Dongsheng Liu,[1,9,*] and Kurt Wüthrich[1,3,5]

## SUMMARY

**Crystal and cryo-EM structures of the glucagon-like peptide-1 receptor (GLP-1R) and glucagon receptor (GCGR) bound with their peptide ligands have been obtained with full-length constructs, indicating that the extracellular domain (ECD) is indispensable for specific ligand binding. This article complements these data with studies of ligand recognition of the two receptors in solution. Paramagnetic NMR relaxation enhancement measurements using dual labeling with fluorine-19 probes on the receptor and nitroxide spin labels on the peptide ligands provided new insights. The glucagon-like peptide-1 (GLP-1) was found to interact with GLP-1R by selective binding to the extracellular surface. The ligand selectivity toward the extracellular surface of the receptor was preserved in the transmembrane domain (TMD) devoid of the ECD. The dual labeling approach further provided evidence of cross-reactivity of GLP-1R and GCGR with glucagon and GLP-1, respectively, which is of interest in the context of medical treatments using combinations of the two polypeptides.**

## INTRODUCTION

Glucagon-like peptide-1 (GLP-1), a peptide hormone containing 31 residues is derived from the tissue-specific posttranslational processing of the proglucagon peptide and inhibits gastric emptying and gut motility through vagal afferents and conveys an anorectic signal to the brain that ultimately reduces food intake.[1–3] GLP-1 functions through activation of the GLP-1 receptor (GLP-1R), a G protein-coupled receptor (GPCR) that is expressed in pancreas, lungs, heart, kidneys, hypothalamus, and stomach. GLP-1R is a class B GPCR and comprises an N-terminal extracellular domain (ECD) and a seven-transmembrane domain (TMD). GLP-1R[TMD] structures in complexes with allosteric modulators, and full length GLP-1R structures in complex with a peptide agonist were solved with X-ray crystallography.[4–6] There are also cryo-EM structures of GLP-1R bound with peptide and non-peptide agonists, positive allosteric modulators, and G proteins.[4–16]

The available structures of GLP-1R have provided snapshots of different activation states and showed that the binding of polypeptide hormone ligands is associated with the ECD. Previous study suggests that activation of GLP-1R is strictly dependent on the presence of ECD.[17] GLP-1R requires the ECD for activation even when high concentration of native peptide is present or when peptide hormones are artificially tethered to the TMD or to the membrane.[17] Physiological ligands had previously been thought not to interact with the GLP-1R[TMD], because no GLP-1R GLP-1 complexes have been detected in the absence of the ECD. Therefore, the question whether TMD alone can interact with GLP-1 and provide selectivity remained unknown. Questions regarding overlaps ("cross-talk") in the interactions among GLP-1R, the glucagon receptor (GCGR), GLP-1, and glucagon (GCG) have been raised and have become major subjects of interest in research on medical treatments using combinations of the two polypeptide hormones.[18]

Here, we employed a dual labeling approach by placing $^{19}$F probes and nitroxide spin labels on the receptor and the peptide ligands, respectively. $^{19}$F-NMR has long been used to characterize weak protein–ligand interactions under equilibrium conditions, owing to its high NMR sensitivity and minimal background.[19–23] In addition, paramagnetic relaxation enhancement (PRE), which is highly sensitive and distance dependent, has been exploited as an NMR method for measuring distances and identifying intermolecular binding partners.[24–28] In this study, we made use of the background-free high resolution of the $^{19}$F-NMR signals

[1]IHuman Institute, ShanghaiTech University, Shanghai 201210, China

[2]University of Chinese Academy of Sciences, Beijing 100049, China

[3]School of Life Science and Technology, ShanghaiTech University, Shanghai 201210, China

[4]Center for Excellence in Molecular Cell Science, Shanghai Institute of Biochemistry and Cell Biology, Chinese Academy of Sciences, Shanghai 200031, China

[5]Department of Integrative Structural and Computational Biology, Scripps Research, La Jolla, CA 92037, USA

[6]Present address: Shanghai Henlius Biotech, Inc., Shanghai 200233, China

[7]Present address: Wuxi Biologics, Shanghai 200131, China

[8]Present address: Department of Rehabilitation, Zhongshan Hospital, Fudan University, Shanghai 200032, China

[9]Lead contact

*Correspondence: liudsh@shanghaitech.edu.cn

https://doi.org/10.1016/j.isci.2023.106918

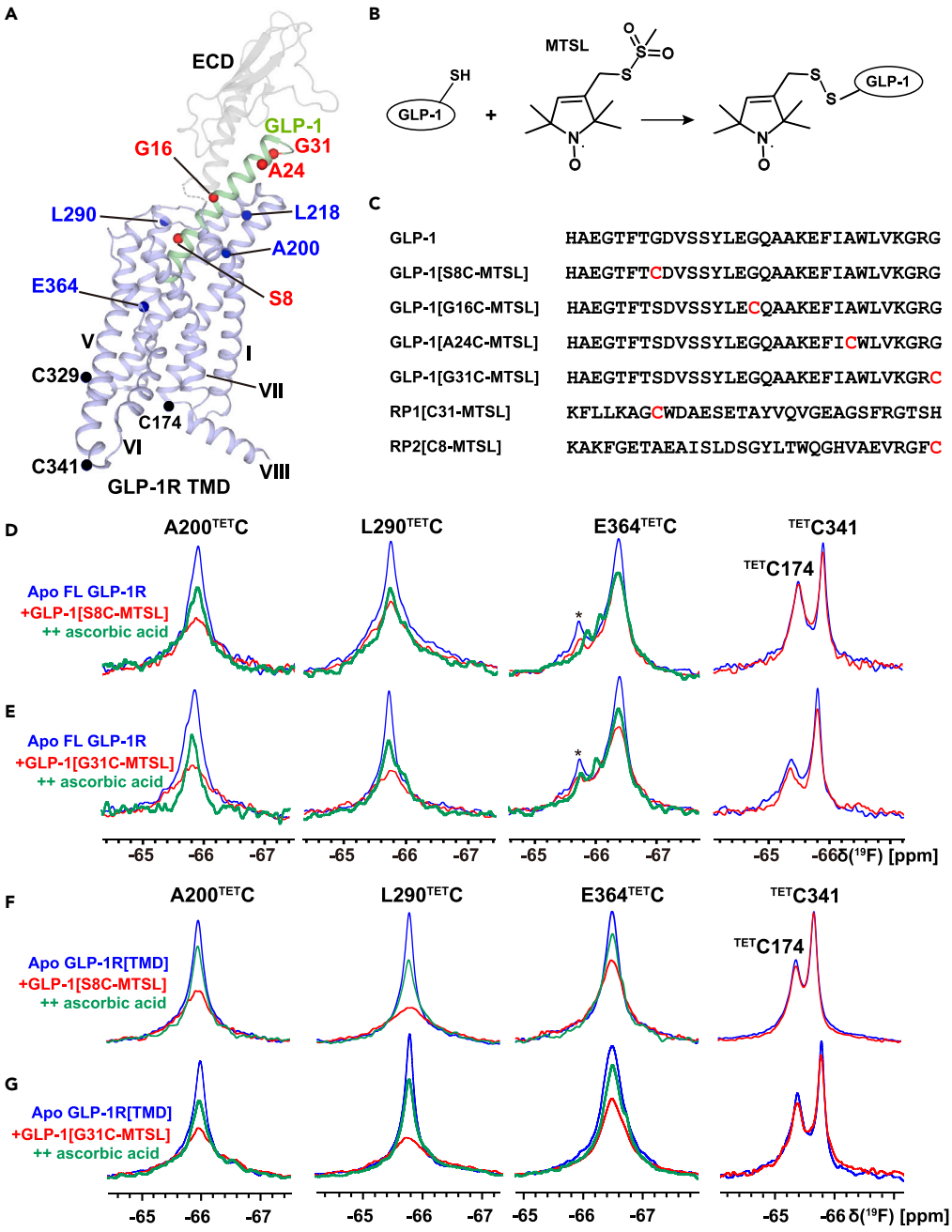


**Figure 1. Selective interactions of the glucagon-like peptide-1 (GLP-1) with the GLP-1R and GLP-1R[TMD]**

(A) Cryo-EM structure of GLP-1R (ECD in gray; TMD in light blue) in complex with GLP-1 (green; PDB:5VAI). The locations of four engineered cysteine labeling sites on the extracellular surface of GLP-1R[TMD] are identified in blue, the locations of three natural cysteines on the intracellular surface of GLP-1R[TMD] are identified in black, and four paramagnetic spin labeling sites in GLP-1 are identified in red.

(B) Chemical reaction used to covalently link the nitroxide spin label, MTSL, to the cysteine residues of GLP-1. MTSL: S-(1-oxyl-2,2,5,5-tetramethyl-2,5-dihydro-1H-pyrrol-3-yl)methyl methanesulfonothioate.

(C) Amino acid sequences of GLP-1, four GLP-1 variants containing engineered cysteines, and two control peptides, RP1 and RP2, with randomized sequences. Engineered cysteines labeled with MTSL are indicated by red letters.

(D and E) Dual-labeling PRE (paramagnetic relaxation enhancement) experiments with $^{19}$F-labeled full length GLP-1R. Three engineered $^{19}$F labeling positions on the extracellular surface (A200$^{TET}$C, L290$^{TET}$C and E364$^{TET}$C) and two natural $^{19}$F labeling positions ($^{TET}$C174 and $^{TET}$C341) on the intracellular surface of GLP-1R were monitored. MTSL-labeled peptide (100 μM) was added to different TET-labeled GLP-1R variants, which were reconstituted in LMNG/CHS micelles.

**Figure 1. *Continued***
The 1D $^{19}$F-NMR spectra were recorded at 298 K on a 600 MHz spectrometer operating at a $^{19}$F resonance frequency of 564 MHz: (D) Addition of GLP-1[S8C-MTSL]; (E) Addition of GLP-1[G31C-MTSL]. Asterisk peak represents nonspecific labeling. FL: full length.
(F and G) Dual-labeling PRE experiments with the GLP-1R[TMD]. Three engineered $^{19}$F labeling positions on the extracellular surface (A200$^{TET}$C, L290$^{TET}$C, and E364$^{TET}$C) and two natural $^{19}$F labeling positions ($^{TET}$C174, $^{TET}$C341) on the intracellular surface of GLP-1R[TMD] were monitored. Spin-labeled GLP-1 (100 μM) was added to the TET-labeled proteins, which were reconstituted in LMNG/CHS micelles. Same experimental conditions and presentation were used for (D) and (E): (F) Addition of GLP-1[S8C-MTSL]; (G) Addition of GLP-1[G31C-MTSL]. The following code is used to present the spectra in the panels (D) to (G): blue, $^{19}$F-NMR signals without the addition of a paramagnetic ligand; red, $^{19}$F-NMR signals after the addition of the MTSL-labeled peptide; green, $^{19}$F-NMR signals after further addition of ascorbic acid to reduce nitroxide radicals. See also Figures S1 and S2 and Table S1.

in the GPCRs and the strong relaxation enhancement because of the nitroxide spin labels in the peptide ligands to characterize weak transient protein–ligand interactions.

## RESULTS

### Selective ligand binding to the extracellular surface of GLP-1R is preserved in the transmembrane domain (TMD)

Our previous studies indicated that three intracellular native cysteines [C174$^{2.44}$, C329$^{5.59}$, and C341; numbers in superscript refer to the Wootten numbering system for class B GPCRs[29]] are subject to 2,2,2-trifluoroethanethiol (TET) labeling[30] and can therefore serve as probes of the intracellular surface of GLP-1R. Four singly engineered cysteine residues (A200$^{2.70}$C, L218C, L290$^{4.66}$C, and E364$^{6.53}$C) were introduced for $^{19}$F-labeling as reporters of the extracellular surface of GLP-1R (Figure 1A). SDS-PAGE and analytical size exclusion chromatography (aSEC) showed that GLP-1R variants reconstituted into lauryl maltose neopentyl glycol/cholesterol hemisuccinate (LMNG/CHS; 5:1) micelles were in good protein yield (0.8–1.0 mg per liter biomass) and homogeneity (Figures S1A and S1E).

Nitroxide spin labels were introduced to GLP-1 to study its interaction with GLP-1R. Site-directed spin labeling was performed by replacing discrete residue positions S8C, G16C, A24C, and G31C on GLP-1, and then labeling with *S*-(1-oxyl-2,2,5,5-tetramethyl-2,5-dihydro-1H-pyrrol-3-yl)methyl methanesulfonothioate (MTSL; Figures 1A–1C). Mass spectrometry (MS) verified the high efficiency of spin-labeling on these peptides (Table S1).

1D $^{19}$F-NMR spectra of GLP-1R[A200$^{TET}$C] and GLP-1R[L290$^{TET}$C] showed a single peak, whereas the spectrum of GLP-1R[E364$^{TET}$C] showed two peaks possibly because of nonspecific labeling (Figures 1D and 1E). GLP-1R[$^{TET}$C174, $^{TET}$C341] showed two separated $^{19}$F-NMR signals corresponding to C174 and C341, respectively.[30] In a typical $^{19}$F-NMR experiment, spin-labeled peptides were added to $^{19}$F-labeled GLP-1R, and the concentrations of the receptor and MTSL-labeled peptide were 15–20 and 100 μM, respectively. The $^{19}$F-NMR signal of A200$^{TET}$C, L290$^{TET}$C, and E364$^{TET}$C on the extracellular surface dropped on the addition of spin-labeled GLP-1, whereas the signals of $^{TET}$C341 and $^{TET}$C174 on the intracellular surface remained almost the same (Figures 1D and 1E). In addition, the partial recovery of $^{19}$F-NMR signals was observed after the addition of 500 μM ascorbic acid to quench nitroxide radicals (Figures 1D and 1E). These results showed that spin-labeled GLP-1 exclusively affected $^{19}$F-NMR signals on the extracellular surface of GLP-1R, but no effect on the intracellular surface signals was detected.

In addition, spin-labeled random peptides were used as non-binder controls in determining whether other spin-labeled peptidic materials can cause signal variations (Figure 1C). Decreases in the intensities of $^{19}$F-NMR signals on the extracellular surface after the addition of RP1[C31-MTSL] were smaller than those observed after the addition of spin-labeled GLP-1 (Figures S2A, 1D and 1E). No effects on the intracellular $^{19}$F-NMR signals were observed (Figure S2A). These experiments indicated that GLP-1R's extracellular surface exhibited greater selectivity to GLP-1 than to other random peptides.

We further performed spin radical 4-hydroxy-2,2,6,6-tetramethyl-piperidinooxy (TEMPOL) titration to explore the solvent exposure of $^{19}$F-labels on the intracellular and extracellular surfaces of the receptor. The $^{19}$F-NMR signals of L290$^{TET}$C, $^{TET}$C329, $^{TET}$C174 and $^{TET}$C341 gradually decreased with increasing TEMPOL concentration (Figure S2B), suggesting the similar solvent-accessibility of the extracellular and intracellular surfaces. A higher concentration (~3 mM) of TEMPOL led to a significant drop in $^{19}$F-NMR

signal intensity, suggesting a strong PRE effect (Figure S2B). Low concentrations (<200 μM) of free radicals caused a minor decrease (<2%) in $^{19}$F-NMR signal intensity, suggesting that the nonspecific interactions of free radicals with the $^{19}$F-probes were minimal.

To investigate whether this selectivity is a property provided by ECD, we further expanded our study to the interaction of GLP-1 with GLP-1R in the absence of ECD (Figures 1F and 1G). The 1D $^{19}$F-NMR spectra of GLP-1R[TMD, A200$^{TET}$C], GLP-1R[TMD, L290$^{TET}$C], GLP-1R[TMD, E364$^{TET}$C], and GLP-1R [TMD, $^{TET}$C174, $^{TET}$C341] all showed a single peak with similar chemical shift as $^{19}$F-NMR signals on GLP-1R but with smaller line width (Figures 1F and 1G). The $^{19}$F-NMR signals of A200$^{TET}$C, L290$^{TET}$C, and E364$^{TET}$C on the extracellular surface dropped significantly on the addition of spin-labeled GLP-1 variants, compared with the almost unchanged intercellular surface signals of $^{TET}$C341 and $^{TET}$C174 (Figures 1F and 1G). We therefore concluded that the TMD devoid of the ECD shows specific interactions of the extracellular surface with GLP-1. Compared with the intracellular surface, the affinity of extracellular surface toward GLP-1 or even a random peptide may reflect the general biophysical or biochemical properties of the receptor.

## Ligand binding selectivity to the extracellular surface is maintained in different membrane mimetics

The ligand binding selectivity of the extracellular surface of GLP-1R[TMD] was next studied in different membrane mimetics: n-dodecyl-b-D-maltopyranosid/cholesterol hemisuccinate (DDM/CHS; 5:1) and nanodiscs (MSP1D1, POPC/POPS ratio of 7:3). SDS-PAGE and aSEC of GLP-1R[TMD, L290$^{TET}$C] and GLP-1R[TMD, $^{TET}$C174, $^{TET}$C341] indicated high protein yields and good homogeneity (Figures S1C, S1D, S1G, and S1H). The 1D $^{19}$F-NMR spectra of GLP-1R[TMD, L290$^{TET}$C], GLP-1R[TMD, $^{TET}$C329], and GLP-1R[TMD, $^{TET}$C174, $^{TET}$C341] titrated by TEMPOL indicated that the extracellular and intracellular surfaces had similar accessibility in LMNG/CHS micelles, DDM/CHS micelles and nanodiscs (Figures 2A–2C and S3D). In the nanodiscs, TEMPOL showed weaker interaction with GLP-1R[TMD] than that in detergent micelles (Figures 2A–2C and S3D), suggesting that the surface of GLP-1R[TMD] is relatively less exposed in the phospholipid bilayer than in the detergent micelles.

In the DDM/CHS micelles, MTSL-labeled GLP-1s selectively broadened the $^{19}$F-NMR peaks on the extracellular surface of GLP-1R[TMD], whereas the intracellular surface signals were less affected (Figures 2E and S3B). Although the effects of $^{19}$F-PRE were much weaker in the nanodiscs, GLP-1 still exclusively affected the NMR signal from the extracellular surface (Figures 2F and S3C). The weaker effects coincided with what we observed in the TEMPOL titration experiments. The bilayer conformation of nanodiscs was possibly much more robust than that of detergent micelles, thus MTSL-labeled peptides and TEMPOL were hindered from getting close to the $^{19}$F-probes. In conclusion, regardless of the membrane mimetics, GLP-1 bound exclusively to the extracellular surface of GLP-1R[TMD] (Figures 2D–2F and S3).

## GLP-1R interactions with polypeptide ligands are weak and reversible

Chemical shift perturbation is generally used to characterize ligand binding effect. The experiment was performed by monitoring $^{19}$F chemical shift changes in response to the titration of the spin labeled ligands. None of the four $^{19}$F-probes near the orthosteric binding pocket showed chemical-shift changes in response to the addition of unlabeled GLP-1(Figure S3A). This results suggest the interaction between GLP-1 and GLP-1R[TMD] is too weak to cause significant chemical shift perturbation. Paramagnetic relaxation enhancement NMR was further used to confirm the finding. A step-by-step titration of GLP-1[G31C-MTSL] into GLP-1R[TMD, L290$^{TET}$C] and GLP-1R[TMD, $^{TET}$C174, $^{TET}$C341] showed that the resonance of L290$^{TET}$C dropped continuously as the concentration of spin labeled peptide increased, whereas the resonance of $^{TET}$C174 and $^{TET}$C341 was less affected (Figures 3A and 3B). The resonance of L290$^{TET}$C could not be saturated even on the addition of 20 times concentration of the ligand (Figure 3A), suggesting the weak interaction between GLP-1 with GLP-1R[TMD] in the detergent micelles.

To verify whether unlabeled GLP-1 can replace the receptor bound labeled GLP-1, competitive binding experiments were employed with the addition of equivalent concentration of unlabeled GLP-1. Results showed that the $^{19}$F-NMR signal of $^{TET}$C290 was partially recovered when unlabeled GLP-1 was added (Figures 3C and 3D), indicating that the binding of unlabeled and labeled GLP-1 to the extracellular surface of the receptor is reversible.

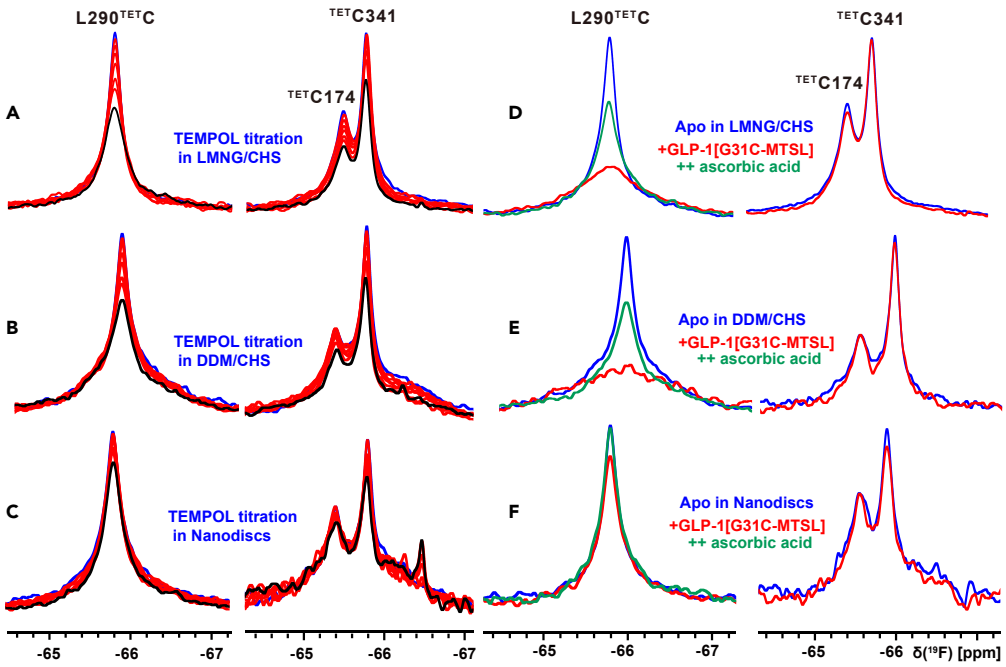


**Figure 2. Solvent accessibility of the GLP-1R[TMD] intracellular and extracellular surface areas and comparison of GLP-1 interactions with GLP-1R[TMD] in different detergent micelles and nanodiscs**

(A–C) Influence of increasing TEMPOL (4-hydroxy-2,2,6,6-tetramethylpiperidinooxy) concentrations (0, 0.1, 0.2, 0.4, 0.8, 1.2, 2, and 3 mM) on the extracellular surface $^{19}$F-NMR signals of GLP-1R[TMD, L290$^{TET}$C] and intracellular surface $^{19}$F-NMR signals of GLP-1R[TMD, $^{TET}$C174, $^{TET}$C341] solubilized in different membrane mimetics: (A) In LMNG/CHS micelles; (B) In DDM/CHS micelles; (C) In nanodiscs. Color code used to present the spectra in the panels (A) to (C): blue, $^{19}$F-NMR signals without the addition of TEMPOL; red, $^{19}$F-NMR signals after the addition of intermediate TEMPOL concentrations (0.1, 0.2, 0.4, 0.8, 1.2, and 2 mM); black, $^{19}$F-NMR signals after the addition of 3 mM TEMPOL.

(D–F) Dual-labeling PRE experiments with $^{19}$F-labeled GLP-1R[TMD] in different membrane mimetics. One engineered $^{19}$F labeling position on the extracellular surface GLP-1R[TMD, L290$^{TET}$C] and two natural $^{19}$F labeling positions on the intracellular surface GLP-1R[TMD, $^{TET}$C174, $^{TET}$C341] were monitored. GLP-1[G31C-MTSL] (100 μM) was added to different TET-labeled proteins. The 1D $^{19}$F-NMR spectra were recorded: (D) in LMNG/CHS micelles; (E) in DDM/CHS micelles; (F) in nanodiscs. Same $^{19}$F-NMR experimental conditions and color code were used as in Figure 1. See also Figure S3.

## Different nitroxide spin label locations in the polypeptide ligands affect its interactions with GLP-1R[TMD]

We further evaluated the effects of discrete peptide labeling position on the selectivity of the extracellular and intracellular surface of the receptor (Figure 1C). Overall, the ligand selectivity of the extracellular surface of the receptor was maintained regardless of peptide labeling position (Figures 4A–4D). Different MTSL labeling position on GLP-1 did cause different degrees of $^{19}$F-NMR signal drop on GLP-1R[TMD]. The C-terminal labeled peptide GLP-1[G31C-MTSL] showed the strongest effect among all peptides (Figure 4D), suggesting GLP-1R[TMD] interact with the C-terminal of peptide stronger than N-terminal. According to the previously structural studies, N-terminal of GLP-1 is buried in the orthosteric binding pocket in TMD whereas the C-terminal of GLP-1 bind to the ECD of in full length GLP-1R. Our results suggest that GLP-1 may adopt different binding modes in GLP-1R and GLP-1R[TMD] in solution. In full-length GLP-1R, the interaction between C-terminal of GLP-1 with ECD maintained the peptide in a canonical position. In the absence ECD, C-terminal of adopted flexible conformation and caused the stronger PRE on the extracellular surface of TMD.

By contrast, RP1[C31-MTSL] and RP2[C8-MTSL] led to similar signal drops on the extracellular surface of GLP-1R[TMD] (Figure S4), suggesting that nonspecific peptide interaction is irrelevant to labeling position. Compared the $^{19}$F-NMR spectra of different labeling positions in GLP-1R[TMD] variants, the position of E364C was less affected by MTSL-labeled polypeptide ligands, suggesting the large distance between E364C and GLP-1. This result was consistent with the cryo-EM structural information that E364 is farther from GLP-1 than the other three extracellular positions.[4–16]

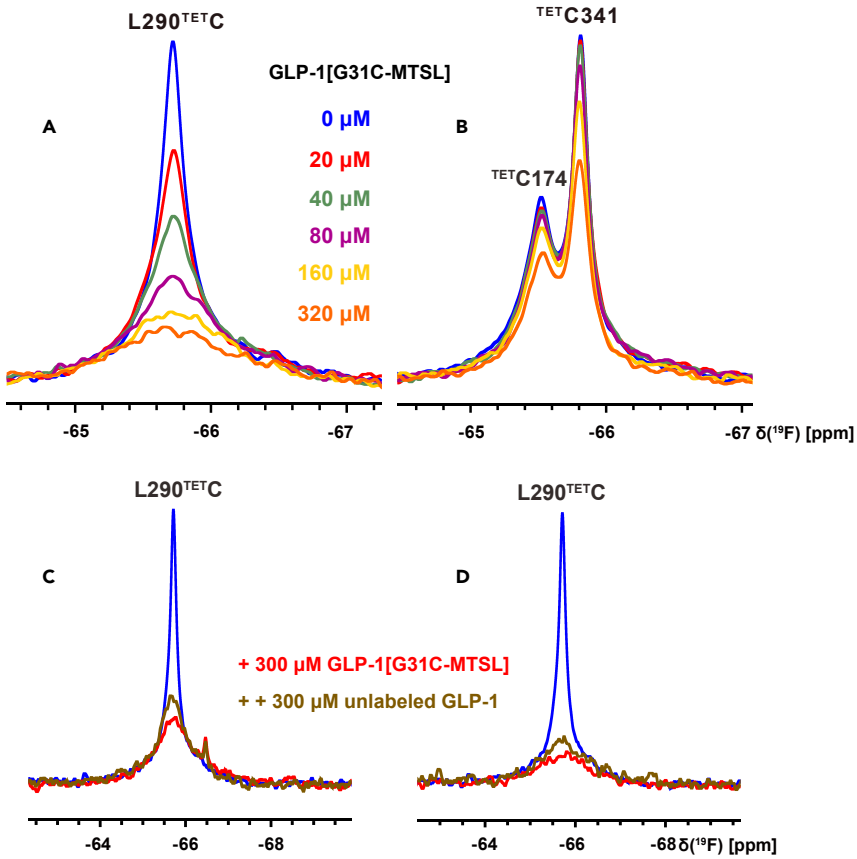


**Figure 3. Weak and reversible interactions between GLP-1 and GLP-1R[TMD]**

(A and B) Titration of GLP-1[G31C-MTSL] to GLP-1R[TMD] variants solubilized in LMNG/CHS micelles. Different concentrations of GLP-1[G31C-MTSL] (0, 20, 40, 80, 160, 320 µM) were added to the different TET-labeled proteins: (A) On the extracellular surface GLP-1R[TMD, L290$^{TET}$C]; (B) On the intracellular surface GLP-1R[TMD, $^{TET}$C174, $^{TET}$C341]. Same $^{19}$F-NMR experimental conditions and presentation as for Figure 1. Color code used to present the spectra in the panels (A) and (B): blue, $^{19}$F-NMR signals without addition of paramagnetic ligand; red, green, purple, yellow, orange represents $^{19}$F-NMR signals after addition of 20, 40, 80, 160, 320 µM GLP-1[G31C-MTSL], respectively.

(C and D) Competition binding of MTSL-labeled GLP-1 and unlabeled GLP-1 with GLP-1R[TMD] in LMNG/CHS micelles. 300 µM MTSL-labeled ligands were added to TET-labeled GLP-1R[TMD, L290$^{TET}$C] and 1D $^{19}$F-NMR spectra were recorded: (C) Addition of GLP-1[S8C-MTSL]; (D) Addition of GLP-1[G31C-MTSL]. Subsequently, 300 µM GLP-1 was added and a second spectrum was recorded. Same $^{19}$F-NMR experimental conditions and presentation as for Figure 1. Color code used to present the spectra in the panels (C) to (D): blue, $^{19}$F-NMR signals without addition of a paramagnetic ligand; red, $^{19}$F-NMR signals after addition of the MTSL-labeled peptide; brown, $^{19}$F-NMR signals after further addition of 300 µM GLP-1.See also Figure S3.

## Cross-reactivity of GLP-1R and GCGR with GLP-1 and GCG

To determine whether the selectivity discovered with GLP-1R is of relevance for class B GPCRs in general, we next extended our study to GCGR and conducted the aforementioned key $^{19}$F-NMR experiments. The GCGR[TMD] constructs were previously described, and extracellular C287$^{4.65}$ and intracellular C171$^{2.44}$ can be readily labeled and used as reporters (Figure 5A).[30]

A mutated version of GCG N28D (GCG*) was used in resolving the solubility issue near the physiological pH.[31] Engineered cysteines on GCG* (F6C, S16C, F22C, and T29C) were next labeled with MTSL, and the products were verified by MS (Figure 5B and Table S1).

Two $^{19}$F-NMR peaks of identical intensity located at −65.4 and −66.2 ppm were assigned to $^{TET}$C287 and $^{TET}$C171, respectively (Figures 5C–5F). Nitroxide spin-labeled GCG peptides decreased the intensity of $^{TET}$C287 signal on the extracellular surface of GCGR[TMD], whereas the signal of $^{TET}$C171 on the

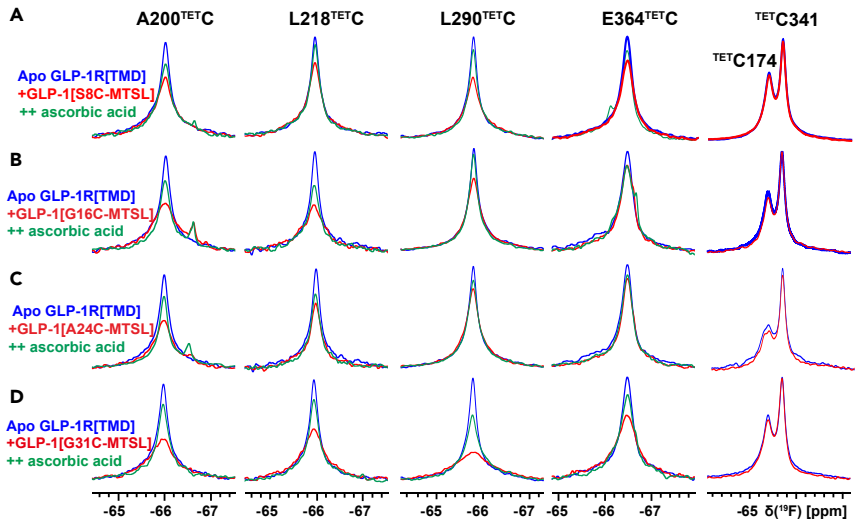


**Figure 4. Interactions of GLP-1R[TMD] variants with spin-labeled GLP-1**

(A–D) Dual-labeling PRE experiments with $^{19}$F-labeled GLP-1R[TMD] in LMNG/CHS micelles. Four engineered $^{19}$F labeling positions on the extracellular surface (A200$^{TET}$C, L218$^{TET}$C, L290$^{TET}$C and E364$^{TET}$C) and two natural $^{19}$F labeling positions ($^{TET}$C174, $^{TET}$C341) on the intracellular surface of GLP-1R[TMD] were monitored. 100 μM MTSL-labeled peptide was added to the different TET-labeled proteins. The 1D $^{19}$F-NMR spectra were recorded: (A) Addition of GLP-1[S8C-MTSL]; (B) Addition of GLP-1[G16C-MTSL]; (C) Addition of GLP-1[A24C-MTSL]; (D) Addition of GLP-1 [G31C-MTSL]. Some figures in Figures 4A and 4D are same with Figures 1F and 1G for convenient comparison. See also Figure S4.

intracellular surface remained unchanged (Figures 5C–5F). Selectivity toward the GCGR extracellular surface was further confirmed in the single labeled variants, GCGR [TMD, $^{TET}$C287] and GCGR [TMD, $^{TET}$C171] (Figures S5I and S5J). This selectivity of the peptidic ligands toward the extracellular surface of

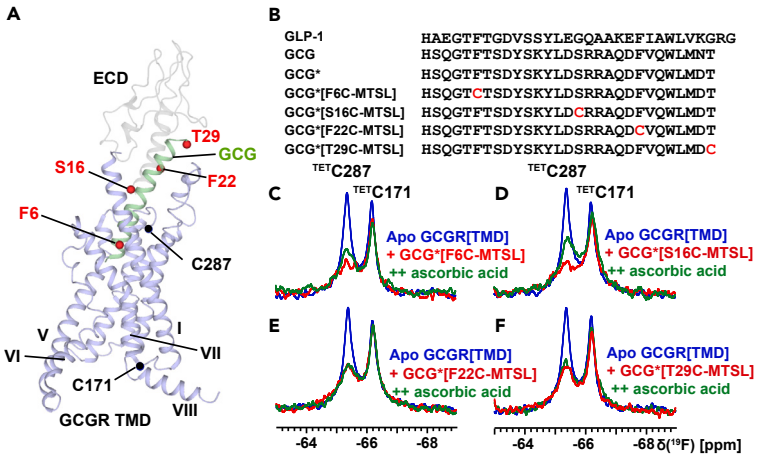


**Figure 5. Selective interactions of GCG with GCGR[TMD]**

(A) Cryo-EM structure of GCGR (ECD in gray, TMD in light blue) in complex with GCG (green) (PDB: 6LML). The locations of two natural cysteine labeling sites of the GCGR[TMD] are identified in black, and four paramagnetic spin labeling sites in GCG* are identified in red. GCG*: GCG[N28D].

(B) Amino acid sequences of GCG, GCG*, and four GCG* variants. Engineered cysteines to be labeled with MTSL are indicated by red letters.

(C–F) Dual-labeling PRE experiments with $^{19}$F-labeled GCGR[TMD]. Two natural cysteine labeling positions on the extracellular and intracellular surface were monitored. MTSL-labeled peptide (100 μM) was added to GCGR[TMD], which was reconstituted in LMNG/CHS micelles. The 1D $^{19}$F-NMR spectra were recorded: (C) Addition of GCG*[F6C-MTSL]; (D) Addition of GCG*[S16C-MTSL]; (E) Addition of GCG*[F22C-MTSL]; (F) Addition of GCG*[T29C-MTSL]. Same $^{19}$F-NMR experimental conditions and color code were used as in Figure 1. See also Figures S1 and S5 and Table S1.

the receptor was preserved in GLP-1R and GCGR in the absence of ECD, suggesting it may be an inherent property of the transmembrane domains of GPCRs.

Of interest, spin-labeled GCG* specifically attenuated the $^{19}$F-NMR signals on the extracellular surface of GLP-1R[TMD] similar to spin-labeled GLP-1 (Figures 6A and S5A–S5D). The selective binding of GCG to the extracellular surface was also observed for full-length GLP-1R (Figures S5E and S5F). In GCGR[TMD], MTSL-labeled GLP-1 caused PRE effects similar to that of the MTSL-labeled GCG*, suggesting that GLP-1 can also bind to GCGR[TMD] as GCG* (Figures S5G and S5H). These results provided clear-cut evidence of the cross-reactivity of GLP-1R and GCGR with their natural ligands.

## DISCUSSION

GPCRs are activated or modulated by a very large set of diverse ligands with chemotypes ranging from small-molecule neurotransmitters, lipids, metabolites and ions, to peptides and small proteins that protrude far beyond the "classical" binding site.[32] NMR studies in solution using dual labeling with $^{19}$F and nitroxide spin labels revealed selective binding of polypeptide hormones to the extracellular surface of the GLP-1R and GCGR TMDs devoid of the ECD (Figures 6A and 6B). Compared with the intracellular binding pocket, which interacts with G-protein, GRK and arrestin, the extracellular loops may play an important role in the diverse signaling ability of the GPCRs. To further explore the molecular mechanism that govern the ligands' selective binding to the extracellular surface of the receptors, we compared the GLP-1R[TMD]

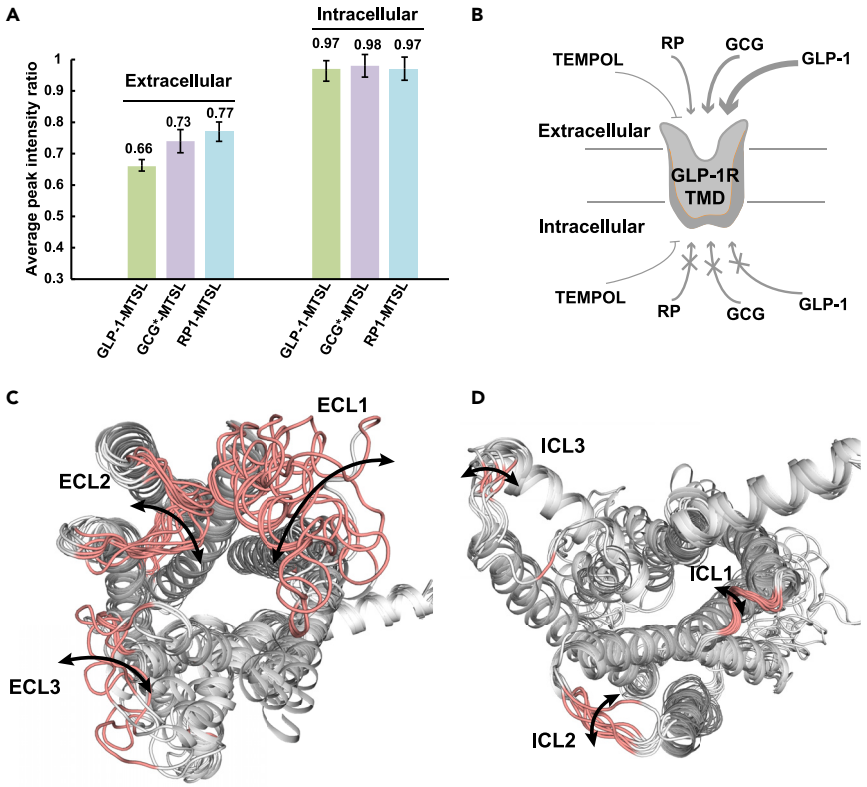


**Figure 6. Selective binding of different polypeptide ligands for the extracellular surface of GLP-1R[TMD]**

(A) PRE effects of MTSL-labeled peptides on the extracellular and intracellular surfaces of the GLP-1R[TMD] in LMNG/CHS micelles. Average peak intensity ratios of the $^{19}$F-NMR signals before and after the addition of MTSL-labeled GLP-1s (green), GCG*s (purple), and RP1 (blue) were calculated according to the data in Figures S5A–S5E and S6A–S6D, respectively. RP: random peptide. Data is represented as mean ± SD of three separate experiments. (B) Model of GLP-1R [TMD] interacting with different types of molecules. Peptide ligands interact selectively with the extracellular surface of GLP-1[TMD]. Small molecules (e.g., TEMPOL) affect both surfaces equally.

(C and D) Comparison of the unstructured loop regions of nine different GLP-1R structures. The models were built based on the crystal and cryo-EM structures with the PDB IDs 7LCI, 7LCK, 6X1A, 6X18, 6X19, 6B3J, 6ORZ, 7C2E, and 5VEW, using SWISS-MODEL (https://swissmodel.expasy.org/): (C) Extracellular view; (D) Intracellular view.

structural models which was made based on the available crystal and cryo-EM structures[5,8,10,11,13,15] (Figures 6C and 6D). Although the transmembrane helices of the TMD superimposed well, the comparison revealed long flexibly disordered extracellular loops (ECLs) with respect to the intracellular loops (ICLs). The current study therefore suggests that the plasticity of extracellular surface should govern the initial stage of ligands recognition and facilitate the ligand binding. The exploitation of these ECL regions may offer the greatest opportunities for developing receptor-specific drugs in the future.

The dual labeling approach is extremely rewarding in detecting the weak, transient intramolecular interactions in solution and can be readily applied to the studies of other membrane proteins. The method also was used for the study of the cross-reactivity of GLP-1R and GCGR with their natural ligands. The therapeutic utility of integrating hormones into a single molecular entity that offers a unique potential for the treatment of diseases.[33] Day et al. showed that when full GLP-1 agonism was augmented with an appropriate degree of GCGR activation, body fat reduction could be substantially enhanced without any overt adverse effects.[34] Finan B et al. demonstrated that the chemical hybridization of GCG and thyroid hormone can optimize the therapeutic effect for metabolic disease.[35] A double-blind, randomized phase 2 study showed that the dual GIP and GLP-1 receptor agonist, LY3298176, had significantly better efficacy with regard to glucose control and weight loss than dulaglutide.[36] LY3298176 (Tirzepatide) was later approved by FDA, for the treatment of adults with type 2 diabetes, making it the first and only GIP and GLP-1 receptor agonist for this indication. The "cross interaction" between these two class B GPCRs and their peptide ligands gave us a new molecular perspective on drug design.

### Limitations of the study

The presently used dual labeling of the ligand-receptor system with $^{19}$F-NMR probes and nitroxide radicals provides novel access to the class B GPCR-ligand interactions in solution. Despite its great potential, the method has its limitations: The labeling itself may perturb the intermolecular interactions, and the micelles selected for solubilizing the GPCR may also affect the results. In addition, the resolution of structural information is limited because of the dependence on long-range interactions between the $^{19}$F spins and the paramagnetic radicals.

## STAR★METHODS

Detailed methods are provided in the online version of this paper and include the following:

- KEY RESOURCES TABLE
- RESOURCE AVAILABILITY
  - Lead contact
  - Materials availability
  - Data and code availability
- EXPERIMENTAL MODEL AND SUBJECT DETAILS
- METHOD DETAILS
  - GPGR constructs
  - Expression, purification and $^{19}$F-labeling of GLP-1R and GCGR in detergent micelles
  - Expression and purification of MSP1D1
  - GPCRs purification and $^{19}$F labeling in nanodiscs
  - MTSL-labeling of polypeptide ligands
  - Mass spectrometry of polypeptide ligands carrying nitroxide spin labels
  - NMR experiments

## SUPPLEMENTAL INFORMATION

Supplemental information can be found online at https://doi.org/10.1016/j.isci.2023.106918.

## ACKNOWLEDGMENTS

D.L. acknowledges funding from the National Natural Science Foundation of China (No. 31971153 and 31670733). K.W. is the Cecil H. and Ida M. Green Professor of Structural Biology at Scripps Research. We thank Profs. Raymond Stevens, Houchao Tao, and Gaojie Song for helpful discussions, Dr. Fei Zhao for help with the HPLC purification of the MTSL-labeled peptides and the MS measurements, and the Cloning,

Insect Cell Expression, Protein Purification and NMR Core Facilities of the iHuman Institute for their support.

## AUTHOR CONTRIBUTIONS

K.W. and D.L. conceived and supervised the study. H.W., D.L., and K.W. designed the experiments. H.W. and W.H. carried out protein production and sample purification and recorded the NMR spectra. H.W., W.H., and T.X. prepared the spin-labeled peptides. Y.Y. and D.L. pursued the initial screenings of the GCGR and GLP-1R expression constructs. H.W., D.L., and K.W. analyzed data and wrote the manuscript with input from all the authors.

## DECLARATION OF INTERESTS

The authors declare no competing interests.

Received: December 8, 2022
Revised: February 27, 2023
Accepted: May 14, 2023
Published: May 19, 2023

## REFERENCES

1. Baggio, L.L., and Drucker, D.J. (2007). Biology of incretins: GLP-1 and GIP. Gastroenterology *132*, 2131–2157. https://doi.org/10.1053/j.gastro.2007.03.054.

2. Drucker, D.J. (2016). The cardiovascular biology of glucagon-like peptide-1. Cell Metabol. *24*, 15–30. https://doi.org/10.1016/j.cmet.2016.06.009.

3. Graaf, C.d., Donnelly, D., Wootten, D., Lau, J., Sexton, P.M., Miller, L.J., Ahn, J.M., Liao, J., Fletcher, M.M., Yang, D., et al. (2016). Glucagon-like peptide-1 and its class B G protein-coupled receptors: a long march to therapeutic successes. Pharmacol. Rev. *68*, 954–1013. https://doi.org/10.1124/pr.115.011395.

4. Jazayeri, A., Rappas, M., Brown, A.J.H., Kean, J., Errey, J.C., Robertson, N.J., Fiez-Vandal, C., Andrews, S.P., Congreve, M., Bortolato, A., et al. (2017). Crystal structure of the GLP-1 receptor bound to a peptide agonist. Nature *546*, 254–258. https://doi.org/10.1038/nature22800.

5. Song, G., Yang, D., Wang, Y., de Graaf, C., Zhou, Q., Jiang, S., Liu, K., Cai, X., Dai, A., Lin, G., et al. (2017). Human GLP-1 receptor transmembrane domain structure in complex with allosteric modulators. Nature *546*, 312–315. https://doi.org/10.1038/nature22378.

6. Wu, F., Yang, L., Hang, K., Laursen, M., Wu, L., Han, G.W., Ren, Q., Roed, N.K., Lin, G., Hanson, M.A., et al. (2020). Full-length human GLP-1 receptor structure without orthosteric ligands. Nat. Commun. *11*, 1272. https://doi.org/10.1038/s41467-020-14934-5.

7. Zhang, Y., Sun, B., Feng, D., Hu, H., Chu, M., Qu, Q., Tarrasch, J.T., Li, S., Sun Kobilka, T., Kobilka, B.K., and Skiniotis, G. (2017). Cryo-EM structure of the activated GLP-1 receptor in complex with a G protein. Nature *546*, 248–253. https://doi.org/10.1038/nature22394.

8. Liang, Y.L., Khoshouei, M., Glukhova, A., Furness, S.G.B., Zhao, P., Clydesdale, L., Koole, C., Truong, T.T., Thal, D.M., Lei, S., et al. (2018). Phase-plate cryo-EM structure of a biased agonist-bound human GLP-1 receptor-Gs complex. Nature *555*, 121–125. https://doi.org/10.1038/nature25773.

9. Kawai, T., Sun, B., Yoshino, H., Feng, D., Suzuki, Y., Fukazawa, M., Nagao, S., Wainscott, D.B., Showalter, A.D., Droz, B.A., et al. (2020). Structural basis for GLP-1 receptor activation by LY3502970, an orally active nonpeptide agonist. Proc. Natl. Acad. Sci. USA *117*, 29959–29967. https://doi.org/10.1073/pnas.2014879117.

10. Zhao, P., Liang, Y.L., Belousoff, M.J., Deganutti, G., Fletcher, M.M., Willard, F.S., Bell, M.G., Christe, M.E., Sloop, K.W., Inoue, A., et al. (2020). Activation of the GLP-1 receptor by a non-peptidic agonist. Nature *577*, 432–436. https://doi.org/10.1038/s41586-019-1902-z.

11. Zhang, X., Belousoff, M.J., Zhao, P., Kooistra, A.J., Truong, T.T., Ang, S.Y., Underwood, C.R., Egebjerg, T., Šenel, P., Stewart, G.D., et al. (2020). Differential GLP-1R binding and activation by peptide and non-peptide agonists. Mol. Cell *80*, 485–500.e7. https://doi.org/10.1016/j.molcel.2020.09.020.

12. Bueno, A.B., Sun, B., Willard, F.S., Feng, D., Ho, J.D., Wainscott, D.B., Showalter, A.D., Vieth, M., Chen, Q., Stutsman, C., et al. (2020). Structural insights into probe-dependent positive allosterism of the GLP-1 receptor. Nat. Chem. Biol. *16*, 1105–1110. https://doi.org/10.1038/s41589-020-0589-7.

13. Ma, H., Huang, W., Wang, X., Zhao, L., Jiang, Y., Liu, F., Guo, W., Sun, X., Zhong, W., Yuan, D., and Xu, H.E. (2020). Structural insights into the activation of GLP-1R by a small molecule agonist. Cell Res. *30*, 1140–1142. https://doi.org/10.1038/s41422-020-0384-8.

14. Johnson, R.M., Zhang, X., Piper, S.J., Nettleton, T.J., Vandekolk, T.H., Langmead, C.J., Danev, R., Sexton, P.M., and Wootten, D. (2021). Cryo-EM structure of the dual incretin receptor agonist, peptide-19, in complex with the glucagon-like peptide-1 receptor. Biochem. Biophys. Res. Commun. *578*, 84–90. https://doi.org/10.1016/j.bbrc.2021.09.016.

15. Zhang, X., Belousoff, M.J., Liang, Y.L., Danev, R., Sexton, P.M., and Wootten, D. (2021). Structure and dynamics of semaglutide- and taspoglutide-bound GLP-1R-Gs complexes. Cell Rep. *36*, 109374. https://doi.org/10.1016/j.celrep.2021.109374.

16. Deganutti, G., Liang, Y.L., Zhang, X., Khoshouei, M., Clydesdale, L., Belousoff, M.J., Venugopal, H., Truong, T.T., Glukhova, A., Keller, A.N., et al. (2022). Dynamics of GLP-1R peptide agonist engagement are correlated with kinetics of G protein activation. Nat. Commun. *13*, 92. https://doi.org/10.1038/s41467-021-27760-0.

17. Zhao, L.H., Yin, Y., Yang, D., Liu, B., Hou, L., Wang, X., Pal, K., Jiang, Y., Feng, Y., Cai, X., et al. (2016). Differential requirement of the extracellular domain in activation of class B G protein-coupled receptors. J. Biol. Chem. *291*, 15119–15130. https://doi.org/10.1074/jbc.M116.726620.

18. Hope, D.C.D., Vincent, M.L., and Tan, T.M.M. (2021). Striking the balance: GLP-1/Glucagon Co-agonism as a treatment strategy for obesity. Front. Endocrinol. *12*, 735019. https://doi.org/10.3389/fendo.2021.735019.

19. Liu, J.J., Horst, R., Katritch, V., Stevens, R.C., and Wüthrich, K. (2012). Biased signaling pathways in beta2-adrenergic receptor characterized by 19F-NMR. Science *335*, 1106–1110. https://doi.org/10.1126/science.1215802.

20. Picard, L.P., and Prosser, R.S. (2021). Advances in the study of GPCRs by (19)F NMR. Curr. Opin. Struct. Biol. *69*, 169–176. https://doi.org/10.1016/j.sbi.2021.05.001.

21. Ge, H., Wang, H., Pan, B., Feng, D., Guo, C., Yang, L., Liu, D., and Wüthrich, K. (2022). G protein-coupled receptor (GPCR) reconstitution and labeling for solution nuclear magnetic resonance (NMR) studies of the structural basis of transmembrane signaling. Molecules *27*, 2658. https://doi.org/10.3390/molecules27092658.

22. Pan, B., Liu, D., Yang, L., and Wüthrich, K. (2022). GPCR large-amplitude dynamics by (19)F-NMR of aprepitant bound to the neurokinin 1 receptor. Proc. Natl. Acad. Sci. USA *119*, e2122682119. https://doi.org/10.1073/pnas.2122682119.

23. Sušac, L., O'Connor, C., Stevens, R.C., and Wüthrich, K. (2015). In-membrane chemical modification (IMCM) for site-specific chromophore labeling of GPCRs. Angew. Chem., Int. Ed. Engl. *54*, 15246–15249. https://doi.org/10.1002/anie.201508506.

24. Mizumura, T., Kondo, K., Kurita, M., Kofuku, Y., Natsume, M., Imai, S., Shiraishi, Y., Ueda, T., and Shimada, I. (2020). Activation of adenosine A(2A) receptor by lipids from docosahexaenoic acid revealed by NMR. Sci. Adv. *6*, eaay8544. https://doi.org/10.1126/sciadv.aay8544.

25. Imai, S., Yokomizo, T., Kofuku, Y., Shiraishi, Y., Ueda, T., and Shimada, I. (2020). Structural equilibrium underlying ligand-dependent activation of beta(2)-adrenoreceptor. Nat. Chem. Biol. *16*, 430–439. https://doi.org/10.1038/s41589-019-0457-5.

26. Clore, G.M., and Iwahara, J. (2009). Theory, practice, and applications of paramagnetic relaxation enhancement for the characterization of transient low-population states of biological macromolecules and their complexes. Chem. Rev. *109*, 4108–4139. https://doi.org/10.1021/cr900033p.

27. Huang, Y., Wang, X., Lv, G., Razavi, A.M., Huysmans, G.H.M., Weinstein, H., Bracken, C., Eliezer, D., and Boudker, O. (2020). Use of paramagnetic (19)F NMR to monitor domain movement in a glutamate transporter homolog. Nat. Chem. Biol. *16*, 1006–1012. https://doi.org/10.1038/s41589-020-0561-6.

28. Matei, E., and Gronenborn, A.M. (2016). 19 F paramagnetic relaxation enhancement: a valuable tool for distance measurements in proteins. Angew. Chem., Int. Ed. Engl. *55*, 150–154. https://doi.org/10.1002/anie.201508464.

29. Wootten, D., Simms, J., Miller, L.J., Christopoulos, A., and Sexton, P.M. (2013). Polar transmembrane interactions drive formation of ligand-specific and signal pathway-biased family B G protein-coupled receptor conformations. Proc. Natl. Acad. Sci. USA *110*, 5211–5216. https://doi.org/10.1073/pnas.1221585110.

30. Wang, H., Hu, W., Liu, D., and Wüthrich, K. (2021). Design and preparation of the class B G protein-coupled receptors GLP-1R and GCGR for (19) F-NMR studies in solution. FEBS J. *288*, 4053–4063. https://doi.org/10.1111/febs.15686.

31. Chabenne, J.R., DiMarchi, M.A., Gelfanov, V.M., and DiMarchi, R.D. (2010). Optimization of the native glucagon sequence for medicinal purposes. J. Diabetes Sci. Technol. *4*, 1322–1331. https://doi.org/10.1177/193229681000400605.

32. Jakowiecki, J., Miszta, P., Niewieczerzał, S., and Filipek, S. (2020). In Chapter 3 - Structural diversity in ligand recognition by GPCRs, GPCRs, B. Jastrzebska, and P.S.H. Park, eds. (Academic Press), pp. 43–63. https://doi.org/10.1016/B978-0-12-816228-6.00003-9.

33. Sadry, S.A., and Drucker, D.J. (2013). Emerging combinatorial hormone therapies for the treatment of obesity and T2DM. Nat. Rev. Endocrinol. *9*, 425–433. https://doi.org/10.1038/nrendo.2013.47.

34. Day, J.W., Ottaway, N., Patterson, J.T., Gelfanov, V., Smiley, D., Gidda, J., Findeisen, H., Bruemmer, D., Drucker, D.J., Chaudhary, N., et al. (2009). A new glucagon and GLP-1 co-agonist eliminates obesity in rodents. Nat. Chem. Biol. *5*, 749–757. https://doi.org/10.1038/nchembio.209.

35. Finan, B., Clemmensen, C., Zhu, Z., Stemmer, K., Gauthier, K., Müller, L., De Angelis, M., Moreth, K., Neff, F., Perez-Tilve, D., et al. (2016). Chemical hybridization of glucagon and thyroid hormone optimizes therapeutic impact for metabolic disease. Cell *167*, 843–857.e14. https://doi.org/10.1016/j.cell.2016.09.014.

36. Frias, J.P., Nauck, M.A., Van, J., Kutner, M.E., Cui, X., Benson, C., Urva, S., Gimeno, R.E., Milicevic, Z., Robins, D., and Haupt, A. (2018). Efficacy and safety of LY3298176, a novel dual GIP and GLP-1 receptor agonist, in patients with type 2 diabetes: a randomised, placebo-controlled and active comparator-controlled phase 2 trial. Lancet *392*, 2180–2193. https://doi.org/10.1016/S0140-6736(18)32260-8.

37. Bayburt, T.H., and Sligar, S.G. (2010). Membrane protein assembly into Nanodiscs. FEBS Lett. *584*, 1721–1727. https://doi.org/10.1016/j.febslet.2009.10.024.

## STAR★METHODS

### KEY RESOURCES TABLE

| REAGENT or RESOURCE | SOURCE | IDENTIFIER |
|---|---|---|
| Bacterial and virus strains | | |
| *E. coli* cells DH5α | TIANGEN | Cat#CB101 |
| *E. coli* cells DH10Bac | 2nd Lab | Cat#DL1071 |
| *E. coli* cells Top10 | TIANGEN | Cat#CB104 |
| *E. coli* cells BL21-Gold (DE3) | TransGen | Cat#CD601-01 |
| Chemicals, peptides, and recombinant proteins | | |
| n-dodecyl-beta-D-maltopyranoside (DDM) | Anatrace | Cat#D310 |
| Laurly Maltose Neopentyl Glycol (LMNG) | Anatrace | Cat#NG310 |
| Cholesterol hemisuccinate (CHS) | Sigma | Cat#C6512-25G |
| 2-Oleoyl-1-palmitoyl-sn-glycero-3-phosphocholine (POPC) | Sigma | Cat#42773-500mg |
| 2-Oleoyl-1-palmitoyl-sn-glycero-3-phospho-L-serine sodium salt (POPS) | Sigma | Cat#51581-100mg |
| 4,4′-dithiodipyridine (4-DPS) | Sigma | Cat#143057-5G |
| NNC0640 | Wuxi AppTec | Cat#EW6341-19-P1 |
| 2,2,2-Trifluoroethanethiol (TET) | Sigma | Cat#374008-10G |
| Hexafluoroacetone trihydrate | Alfa Aesar | Cat#L10777.06 |
| 4-hydroxy-2,2,6,6-tetramethyl-piperidinooxy (TEMPOL) | Alfa Aesar | Cat#A12497.03 |
| S-(1-oxyl-2,2,5,5-tetramethyl-2,5-dihydro-1H-pyrrol-3-yl)methyl methanesulfonothioate (MTSL) | Santa Cruz | Cat#SC-208677A |
| Ascorbic acid | Aladdin | Cat#A103534-100g |
| 3-(trimethylsilyl)-1-propanesulfonic acid sodium salt (DSS) | Aldrich | Cat#178837-1G |
| Phusion HF DNA Polymerase | New England Biolabs | Cat#M0503S |
| Dpn1 | New England Biolabs | Cat#R0176L |
| Protease Inhibitor Cocktail | Bimake | Cat#B14003 |
| TALON Superflow Metal Affinity Resin | TAKARA | Cat#635670 |
| Bio-Beads SM-2 Adsorbent Media | Bio-Rad | Cat#152-3920 |
| GLP-1[S8C] | Genscript | C2906DD130-1 |
| GLP-1[G16C] | Genscript | C4509DD230-4 |
| GLP-1[A24C] | Genscript | C4509DD230-5 |
| GLP-1[G31C] | Genscript | C2906DD130-2 |
| GCG*[F6C] | Genscript | C2906DD130-3 |
| GCG*[S16C] | Genscript | C4509DD230-6 |
| GCG*[F22C] | Genscript | C2906DD130-4 |
| GCG*[T29C] | Genscript | C4509DD230-7 |
| RP2[C8] | Genscript | C873UEH260 |
| RP1[C31] | Genscript | C773LFA290-1 |
| GLP-1 | Genscript | C5725BK080 |
| Experimental models: Cell lines | | |
| Insect: Sf9 | Expression Systems | Cat#11496015 |
| Oligonucleotides | | |
| Primer: GLP-1R-C329S-Forward: TTCGTGAGGGTCATCTCTATTGTT GTGAGTAAGCTG | This paper | N/A |

(*Continued on next page*)

*Continued*

| REAGENT or RESOURCE | SOURCE | IDENTIFIER |
|---|---|---|
| Primer: GLP-1R-C329S-Reverse: CTTACTCACAACAATAGAGAT GACCCTCACGAAGAT | This paper | N/A |
| Primer: GLP-1R-A200C-Forward: TTCATTAAGGACG CTTGCCTGAAATGGATGTACTC | This paper | N/A |
| Primer: GLP-1R-A200C-Reverse: GTACATCCATTTCAGGCAAGCGTCCTTAATGAACA | This paper | N/A |
| Primer: GLP-1R-L218C-Forward: TGGGACGGACTCTTGAGCTACCAAGATAGTCTCTC | This paper | N/A |
| Primer: GLP-1R-L218C-Reverse: GAGACTATCTTGGTAGCTCAAGAGTCCGTCCCACT | This paper | N/A |
| Primer: GLP-1R-L290C Forward: GGAATCGTCAAGTACCTGTACGAGGATGAAGGTTG | This paper | N/A |
| Primer: GLP-1R-L290C-Reverse: ACCTTCATCCTCGTACAGGTACTTGACGATTCCCC | This paper | N/A |
| Primer: GLP-1R-E364C-Forward: CTGTGTACGCACGAGGTTATTTTCGCTTTCGTGAT | This paper | N/A |
| Primer: GLP-1R-E364C-Reverse: CACGAAAGCGAAAATAACCTCGTGCGTACACAGCA | This paper | N/A |
| Primer: GCGR-C171S-Forward: CTGTCCAAACTCCAC AGCACTAGAAACGCCATCCA | This paper | N/A |
| Primer: GCGR-C171S-Reverse: GATGGCGTTTCTAGTG CTGTGGAGTTTGGACAGGC | This paper | N/A |
| Primer: GCGR-C287S-Forward: ATTGTCGCTAACTACA GTTGGCTTTTGGTTGAGGG | This paper | N/A |
| Primer: GCGR-C287S-Reverse: CTCAACCAAAAGCCAA CTGTAGTTAGCGACAATT | This paper | N/A |
| Primer: GCGR-C401V-Forward: GTGGCCGTACTGTACG TTTTTCTGAACAAGGAAGT | This paper | N/A |
| Primer: GCGR- C401V-Reverse: TTCCTTGTTCAGAAAAA CGTACAGTACGGCCACGA | This paper | N/A |
| **Recombinant DNA** | | |
| pFastbac1-GLP-1R[TMD] | This paper | N/A |
| pFastbac1-GLP-1R[TMD,C174S,C341S,C329S,A200C] | This paper | N/A |
| pFastbac1-GLP-1R[TMD,C174S,C341S] | This paper | N/A |
| pFastbac1-GLP-1R[TMD,C174S,C341S,C329S,L218C] | This paper | N/A |
| pFastbac1-GLP-1R[TMD,C174S,C341S,C329S,L290C] | This paper | N/A |
| pFastbac1-GLP-1R[TMD,C174S,C341S,C329S,E364C] | This paper | N/A |
| pFastbac1-wtGCGR[TMD] | This paper | N/A |
| pFastbac1-wtGCGR[TMD,C171S,C401V] | This paper | N/A |
| pFastbac1-wtGCGR[TMD,C287S,C401V] | This paper | N/A |
| pFastbac1-wtGCGR[TMD,C287S,C171S] | This paper | N/A |
| **Software and Algorithms** | | |
| TopSpin 3.6.1 | Bruker BioSpin | www.bruker.com |
| PyMOL 2.2.3 | Schrödinger | www.pymol.org |
| OriginPro 2019 | OriginLab | www.originlab.com |
| Adobe Illustrator CC 2018 | Adobe | www.adobe.com |

## RESOURCE AVAILABILITY

### Lead contact

Further information and requests for resources and reagents should be directed to and will be fulfilled by the lead contact, Dongsheng Liu (liudsh@shanghaitech.edu.cn).

### Materials availability

This study did not generate new or unique reagents.

### Data and code availability

- All data reported in this paper will be shared by the lead contact upon request.
- This paper does not report original code.
- Any additional information required to reanalyze the data reported in this paper is available from the lead contact upon request.

## EXPERIMENTAL MODEL AND SUBJECT DETAILS

A pET-28a vector containing the MSP1D1 gene construct was transformed into BL21-Gold (DE3) competent cells for growth and expression. Cultures were grown at 37 °C.

For GLP-1R and GCGR, recombinant baculoviruses were generated by transfecting recombinant bacmids into *Spodoptera frugiperda* (Sf9) cells, using X-tremeGENE HP DNA Transfection Reagent (Roche, Basel, Switzerland) and Transfection Medium (Expression Systems, Davis, CA, USA). Recombinant baculoviruses were amplified using the Bac-to-Bac system (Invitrogen, Carlsbad, CA, USA). Cultures were grown at 27 °C.

## METHOD DETAILS

### GPGR constructs

The original human GLP-1R, GLP-1R[TMD] and GCGR[TMD] constructs used in this study were derived from previous study.[30] In brief, the original GLP-1R[TMD] construct contains six mutations, including an engineered disulfide bond ($I317^{5.47}C$-$G361^{6.5o}C$) linking helices V and VI and four other mutations (S271A, G318I, K346A, C347F). This construct also contains truncations at the amino and carboxy termini, a hemagglutinin (HA) signal sequence, FLAG tag, N-terminal 10× histidine tag, and *Escherichia coli* apocytochrome b562RIL (BRIL), followed by a tobacco etch virus (TEV) protease cleavage site. To place probes on the extracellular surface, C174, C329 and C341 on the intracellular surface were mutated to Ser using the QuikChange site-directed mutagenesis method. Then four point mutations (A200C, L218C, L290C, and V364C) near the orthosteric binding site on extracellular surface were introduced using the QuikChange site-directed mutagenesis method to prepare the $^{19}$F-NMR amenable samples. Residues from 24 to 127 (ECD domain) were added to N-terminal of TMD to build full length GLP-1R construct using standard QuikChange method. The human GCGR[TMD] construct (residue 123-432) contains a N-terminal HA signal sequence, Flag tag, and BRIL, followed by a 10× histidine tag, and a PreScission protease (PPase) cleavage site.

### Expression, purification and $^{19}$F-labeling of GLP-1R and GCGR in detergent micelles

GPCRs were expressed using the Bac-to-Bac system (Invitrogen) in *Spodoptera frugiperda (Sf9)* cells for 48 h. Insect cell pellets were thawed and washed repeatedly twice in hypotonic buffer (10 mM HEPES pH 7.5, 10 mM $MgCl_2$, 20 mM KCl) and three times in high osmotic buffer (1 M NaCl, 10 mM HEPES (pH 7.5), 10 mM $MgCl_2$, 20 mM KCl). The washed membrane was suspended in the hypotonic buffer with inhibitor cocktail and incubated with 1 mM cysteine-activating reagent 4,4′-dithiodipyridine (4-DPS, Sigma) at 4 °C for 1 h. Afterward, excess 4-DPS was removed by washed once again in the high osmotic buffer. Receptor-containing membranes were again suspended in the hypotonic buffer and incubated with 1 mM TET at 4°C for 1 h (Sigma). The membranes were then solubilized with 500 mM NaCl, 50 mM HEPES (pH 7.5), 1 mM 4-DPS, 1% (w/v) LMNG (Anatrace), and 0.2% (w/v) CHS (Sigma-Aldrich) at 4°C for 3 h. The supernatant was isolated by ultracentrifugation and incubated with TALON IMAC resin (Clontech) and 20 mM imidazole at 4°C overnight. The resin was washed with 15 column volumes of washing buffer 1 (50 mM HEPES, pH 7.5, 500 mM NaCl, 30 mM imidazole and 0.01% [w/v] LMNG, 0.002% [w/v] CHS) and 10 column volumes of washing buffer 2 (25 mM HEPES, pH 7.5, 500 mM NaCl, 20 mM imidazole and 0.001% [w/v] LMNG,

0.0002% [w/v] CHS). Subsequently, the resin was resuspended with 2 column volumes of washing buffer 2 in the presence of protease (PPase for GCGR, TEV protease for GLP-1R, molar ratio of 1:20) and incubated at 4°C overnight. The protein was collected from the flow-through of the resin washing buffer 2. Finally, the collected protein was concentrated and exchanged into 20 mM sodium phosphate buffer (pH 7.6), 100 mM KCl, 1 mM EDTA, 20 μM hexafluoroacetone trihydrate, 100 μM sodium 3-(trimethylsilyl)propane-1-sulfonate (DSS) with a 50 kDa cutoff concentrator (Millipore) for NMR experiments. The protein yield and monodispersity were tested by analytical size exclusion chromatography (aSEC). GLP-1R[TMD] in *n*-dodecyl-β-D-maltopyranoside (DDM/CHS) micelles, GLP-1R and GCGR[TMD] in LMNG/CHS micelles were prepared using the aforementioned method but 200 μM NNC0640 was added to stabilize the protein during the purification process.

Analytical SEC is used to calculate the final protein yield. aSEC column was prepared and specified for characterization of purified GPCR in mixed micelles. The column was first washed with SEC running buffer (25 mM HEPES, pH 7.5, 500 mM NaCl, 2% Glycerol, 0.05% LMNG, 0.01% CHS) at 0.5 mL/min until the curve being flat. Bovine Serum Albumin (BSA) samples at different amount (1 μg, 5 μg, 25 μg, etc.) were loaded to make the standard calibration curve (peak height or peak area versus BSA quantity). Then GPCR samples were loaded into aSEC column at ta flow rate of0.5 mL/min. The total GPCR expression yield were calculated from the A280 absorbance based on the standard BSA calibration curve.

### Expression and purification of MSP1D1

The preparations of membrane scaffold protein (MSP) 1D1[37] for nanodiscs were performed using the same procedure as described before.[30] A pET-28a vector containing the MSP1D1 gene construct was transformed into BL21-Gold (DE3) competent cells for growth and expression. The cell cultures were induced with 1 mM IPTG when the OD600 reached 0.6–0.8. The cells were harvested and resuspended in lysis buffer (20 mM PBS, 1% Triton X-100, 1 mM PMSF, pH 7.4). After sonication, the lysate was cleared and loaded onto $Ni^{2+}$ NTA-agarose resin. The $Ni^{2+}$ column was then washed sequentially with the following buffer: (a) 40 mM Tris/HCl, 0.3 M NaCl, 1% Triton X-100, pH 8.0; (b) 40 mM Tris/HCl, 0.3 M NaCl, 50 mM cholate, 20 mM imidazole, pH 8.0; and (c) 40 mM Tris/HCl, 0.3 M NaCl, 50 mM imidazole, pH 8.0. Last, MSP1D1 was eluted and buffer-exchanged or dialyzed using a 7 kD cutoff membrane. Subsequently, TEV protease (molar ratio of 1 : 20) was added to the dialyzed protein and incubated at 4°C overnight. The protein was then loaded again onto a $Ni^{2+}$ column and collected from the flow-through. Finally, the protein was concentrated with 10 kD cutoff concentrators and stored at −80°C.

### GPCRs purification and $^{19}F$ labeling in nanodiscs

The preparations of GLP-1R[TMD] in nanodiscs were performed using the same procedure as described before.[30] In brief, the proteins were labeled with TET, using the in-membrane chemical modification (IMCM) method and then purified with TALON IMAC resin in LMNG/CHS micelles.[23] Then MSP1D1, 1-palmitoyl-2-oleoyl-*sn*-glycero-3-phosphocholine (POPC), and 1-palmitoyl-2-oleoyl-sn-glycero-3-phospho-l-serine (POPS) were added to reach a receptor : MSP1D1 : POPC : POPS molar ratio of 1 : 5 : 245 : 105. This was followed by overnight removal of the detergents with biobeads at 4 °C. After ultracentrifugation, the supernatant was purified again using the $Ni^{2+}$ column to remove the empty nanodiscs. Subsequently, TEV protease was used to cleave the N-terminal fusion partners from the receptors. The $Ni^{2+}$ column was then used again to obtain the final product.

### MTSL-labeling of polypeptide ligands

The peptide variants with engineered cysteines were synthesized and commercially obtained (GenScript). The peptide variants were dissolved in sterile water and incubated with twice concentration MTSL at 4°C for 2 h. After centrifugation at 14000*g* for 30 min, the supernatant was subjected to high-performance liquid chromatography (HPLC)-C18 reverse phase column (ZORBAX StableBond 300C18, 9.4 × 250 mm, 5 μm, Agilent) on the Shimadzu LC-20A HPLC system (Shimadzu Corporation, Kyoto, Japan). The collected purified peptides were lyophilized and stored for future use.

### Mass spectrometry of polypeptide ligands carrying nitroxide spin labels

All liquid chromatography (LC)-MS experiments were performed on Agilent 6230 Accurate-Mass TOF (time-of-flight) LC-MS system. TOF was operated with an orthogonal electrospray source in positive ion mode. The mobile phase was programmed as 0.1% formic acid/acetonitrile (80:20, v/v) at the beginning

and 60:40 at 20 min. The drying gas (nitrogen) temperature was set at 350°C, flow at 10 L/min, nebulizer pressure at 50 psi and capillary voltage (Vcap) at 4000 V. The fragmentor voltage was 100 V. The ions of *m/z* 121.050873 and 922.009798 were used as references. Purine and fluorine compound solutions were always introduced into the ion source, and real-time mass adjustment was performed.

### NMR experiments

NMR samples of GLP-1R, GCGR and variants thereof were prepared with 20 mM sodium phosphate buffer (pH 7.6), 100 mM KCl, 1 mM EDTA, 20 μM hexafluoroacetone, 100 μM sodium 3-(trimethylsilyl)propane-1-sulfonate (DSS) and 10% $D_2O$. Subsequently, MTSL-labeled peptides were added or titrated directly to the receptor samples. For a typical $^{19}$F-NMR experiment, the concentrations of the receptors and MTSL-labeled peptide were 15–20 μM and 100 μM, respectively. Ascorbic acid was added to a final concentration of 500 μM to quench the nitroxide spin label. $^{19}$F-NMR spectra were recorded on a Bruker AVANCE III HD 600 MHz spectrometer equipped with a TCI $^{1}$H/$^{19}$F-$^{13}$C-$^{15}$N triple resonance cryoprobe with shielded z-gradient coil. The $^{19}$F chemical shifts were calibrated using the internal reference hexafluoroacetone at −82.2 ppm. The 1D $^{19}$F-NMR experiments were recorded at 298 K with a data size of 8 k complex points and an acquisition time of 144 ms. Prior to Fourier transformation, 1D $^{19}$F-NMR datasets were zero-filled in the time domain to twice the measured size, and the expanded free induction decays were multiplied using an exponential function with a 30 Hz line-broadening factor.